Groundwater storage dynamics in the world's large aquifer systems from GRACE: uncertainty and role of extreme precipitation

Mohammad Shamsudduha[1,2,*] and Richard G. Taylor[1]

[1] Department of Geography, University College London, London, UK

[2] Department of Geography, University of Sussex, Falmer, Brighton, UK

[*] Corresponding author: M. Shamsudduha (M.Shamsudduha@sussex.ac.uk)

Abstract

Under variable and changing climates groundwater storage sustains vital ecosystems and enables freshwater withdrawals globally for agriculture, drinking-water, and industry. Here, we assess recent changes in groundwater storage (ΔGWS) from 2002 to 2016 in 37 of the world's large aquifer systems using an ensemble of datasets from the Gravity Recovery and Climate Experiment (GRACE) and Land Surface Models (LSMs). Ensemble GRACE-derived ΔGWS is well reconciled to in-situ observations (r = 0.62–0.86, p value <0.001) for two tropical basins with regional piezometric networks and contrasting climate regimes. Trends in GRACE-derived ΔGWS are overwhelmingly non-linear; indeed, linear declining trends adequately (R^2 >0.5, p value <0.001) explain variability in only two aquifer systems. Non-linearity in ΔGWS derives, in part, from the episodic nature of groundwater replenishment associated with extreme annual (>90th percentile, 1901–2016) precipitation and is inconsistent with prevailing narratives of global-scale groundwater depletion at the scale of GRACE footprint (~200,000 km^2). Substantial uncertainty remains in estimates of GRACE-derived ΔGWS, evident from 20 realisations presented here, but these data provide a regional context to changes in groundwater storage observed more locally through piezometry.

1 Introduction

Groundwater is estimated to account for between a quarter and a third of the world's annual freshwater withdrawals to meet agricultural, industrial and domestic demand (Döll et al., 2012; Wada et al., 2014; Hanasaki et al., 2018). As the world's largest distributed store of freshwater, groundwater plays a vital role in sustaining ecosystems and enabling adaptation to increased variability in rainfall and river discharge brought about by climate change (Taylor et al., 2013a). Sustained reductions in the volume of groundwater (i.e. groundwater depletion) resulting from human withdrawals or changes in climate have historically been observed as declining groundwater levels recorded in wells (Scanlon et al., 2012a; Castellazzi et al., 2016; MacDonald et al., 2016). The limited distribution and duration of piezometric records hinder, however, direct observation of changes in groundwater storage globally including many of the world's large aquifer systems (WHYMAP and Margat, 2008).

Since 2002 the Gravity Recovery and Climate Experiment (GRACE) has enabled large-scale ($\geq$ 200,000 km^2) satellite monitoring of changes in total terrestrial water storage (ΔTWS) globally (Tapley et al., 2004). As the twin GRACE satellites circle the globe ~15 times a day they measure the inter-satellite distance at a minute precision (within one micron) and provide ΔTWS for the entire earth approximately every 30 days. GRACE satellites sense movement of total terrestrial water mass derived from both natural (e.g. droughts) and anthropogenic (e.g. irrigation) influences globally (Rodell et al., 2018). Changes in groundwater storage (GRACE-derived ΔGWS) are computed from ΔTWS after deducting contributions (equation 1) that arise from other terrestrial water stores including soil moisture storage (ΔSMS), surface water storage (ΔSWS), and the snow water storage (ΔSNS) using data from Land Surface Models (LSMs) either exclusively (Rodell et al., 2009; Famiglietti et al., 2011; Scanlon et al., 2012a; Famiglietti and Rodell, 2013; Richey et al., 2015; Thomas et

al., 2017) or in combination with in situ observations (Rodell et al., 2007; Swenson et al., 2008; Shamsudduha et al., 2012).

$$\Delta GWS = \Delta TWS - (\Delta SMS + \Delta SWS + \Delta SNS) \quad (1)$$

Substantial uncertainty persists in the quantification of changes in terrestrial water stores from GRACE measurements that are limited in duration (2002 to 2016), and the application of uncalibrated, global-scale LSMs (Shamsudduha et al., 2012; Döll et al., 2014; Scanlon et al., 2018). Computation of ΔGWS from GRACE ΔTWS is argued, nevertheless, to provide evaluations of large-scale changes in groundwater storage where regional-scale piezometric networks do not currently exist (Famiglietti, 2014).

Previous assessments of changes in groundwater storage using GRACE in the world's 37 large aquifer systems (Richey et al., 2015; Thomas et al., 2017) (Fig. 1, Table 1) have raised concerns about the sustainability of human use of groundwater resources. One analysis (Richey et al., 2015) employed a single GRACE ΔTWS product (CSR) in which changes in subsurface storage (ΔSMS + ΔGWS) were attributed to ΔGWS. This study applied linear trends without regard to their significance to compute values of GRACE-derived ΔGWS over 11 years from 2003 to 2013, and concluded that the majority of the world's aquifer systems (n = 21) are either "overstressed" or "variably stressed". A subsequent analysis (Thomas et al., 2017) employed a different GRACE ΔTWS product (Mascons) and estimated ΔSWS from LSM data for both surface and subsurface runoff, though the latter is normally considered to be groundwater recharge (Rodell et al., 2004). Using performance metrics normally applied to surface water systems including dams, this latter analysis classified nearly a third (n = 11) of the world's aquifer systems as having their lowest sustainability criterion.

72 Here, we update and extend the analysis of ΔGWS in the world's 37 large aquifer systems
73 using an ensemble of three GRACE ΔTWS products (CSR, Mascons, GRGS) over a 14-year
74 period from August 2002 to July 2016. To isolate GRACE-derived ΔGWS from GRACE
75 ΔTWS, we employ estimates of ΔSMS, ΔSWS and ΔSNS from five LSMs (CLM, Noah,
76 VIC, Mosaic, Noah v.2.1) run by NASA's Global Land Data Assimilation System (GLDAS).
77 As such, we explicitly account for the contribution of ΔSWS to ΔTWS, which has been
78 commonly overlooked (Rodell et al., 2009; Richey et al., 2015; Bhanja et al., 2016) despite
79 evidence of its significant contribution to ΔTWS (Kim et al., 2009; Shamsudduha et al.,
80 2012; Getirana et al., 2017). Further, we characterise trends in time-series records of
81 GRACE-derived ΔGWS by employing a non-parametric, Seasonal-Trend decomposition
82 procedure based on Loess (STL) (Cleveland et al., 1990) that allows for resolution of
83 seasonal, trend and irregular components of GRACE-derived ΔGWS for each large aquifer
84 system. In contrast to linear or multiple-linear regression-based techniques, STL assumes
85 neither that data are normally distributed nor that the underlying trend is linear
86 (Shamsudduha et al., 2009; Humphrey et al., 2016; Sun et al., 2017).

87

88 ## 2 Data and Methods

89 ### 2.1 Global large aquifer systems

90 We use the World-wide Hydrogeological Mapping and Assessment Programme (WHYMAP)
91 Geographic Information System (GIS) dataset for the delineation of world's 37 Large Aquifer
92 Systems (Fig. 1, Table1) (WHYMAP and Margat, 2008). The WHYMAP network, led by
93 the German Federal Institute for Geosciences and Natural Resources (BGR), serves as a
94 central repository and hub for global groundwater data, information, and mapping with a goal
95 of assisting regional, national, and international efforts toward sustainable groundwater

management (Richts et al., 2011). The largest aquifer system in this dataset (Supplementary Table S1) is the East European Aquifer System (WHYMAP no. 33; area: 2.9 million km^2) and the smallest one the California Central Valley Aquifer System (WHYMAP no. 16; area: 71,430 km^2), which is smaller than the typical sensing area of GRACE (~200,000 km^2). However, Longuevergne et al. (2013) argue that GRACE satellites are sensitive to total mass changes at a basin scale so ΔTWS measurements can be applied to smaller basins if the magnitude of temporal mass changes is substantial due to mass water withdrawals (e.g., intensive groundwater-fed irrigation). Mean and median sizes of these large aquifers are ~945,000 km^2 and ~600,000 km^2, respectively.

2.2 GRACE products

We use post-processed, gridded (1° × 1°) monthly GRACE TWS data from CSR land (Landerer and Swenson, 2012) and JPL Global Mascon (Watkins et al., 2015; Wiese et al., 2016) solutions from NASA's dissemination site (http://grace.jpl.nasa.gov/data), and a third GRGS GRACE solution (CNES/GRGS release RL03-v1) (Biancale et al., 2006) from the French Government space agency, Centre National D'études Spatiales (CNES). To address the uncertainty associated with different GRACE processing strategies (CSR, JPL-Mascons, GRGS), we apply an ensemble mean of the three GRACE solutions (Bonsor et al., 2018).

CSR land solution (version RL05.DSTvSCS1409) is post-processed from spherical harmonics released by the Centre for Space Research (CSR) at the University of Texas at Austin. CSR gridded datasets are available at a monthly timestep and a spatial resolution of 1° × 1° (~111 km at equator) though the actual spatial resolution of GRACE footprint (Scanlon et al., 2012a) is 450 km × 450 km or ~200,000 km^2. To amplify TWS signals we apply the dimensionless scaling factors provided as 1° × 1° bins that are derived from minimising differences between TWS estimated from GRACE and the hydrological fields

from the Community Land Model (CLM4.0) (Landerer and Swenson, 2012). JPL-Mascons (version RL05M_1.MSCNv01) data processing involves the same glacial isostatic adjustment correction but applies no spatial filtering as JPL-RL05M directly relates inter-satellite range-rate data to mass concentration blocks (Mascons) to estimate monthly gravity fields in terms of equal area 3° × 3° mass concentration functions in order to minimise measurement errors. Gridded mascon fields are provided at a spatial sampling of 0.5° in both latitude and longitude (~56 km at the equator). Similar to CSR product, dimensionless scaling factors are provided as 0.5° × 0.5° bins (Shamsudduha et al., 2017) to apply to the JPL-Mascons product that also derive from the Community Land Model (CLM4.0) (Wiese et al., 2016). The scaling factors are multiplicative coefficients that minimize the difference between the smoothed and unfiltered monthly ΔTWS variations from the CLM4.0 hydrology model (Wiese et al., 2016). Finally, GRGS GRACE (version RL03-v1) monthly gridded solutions of a spatial resolution of 1° × 1° are extracted and aggregated time-series data are generated for each aquifer system. A description of the estimation method of ΔGWS from GRACE and in-situ observations is provided below.

2.3 Estimation of ΔGWS from GRACE

We apply monthly measurements of terrestrial water storage anomalies (ΔTWS) from Gravity Recovery and Climate Experiment (GRACE) satellites, and simulated records of soil moisture storage (ΔSMS), surface runoff or surface water storage (ΔSWS) and snow water equivalent (ΔSNS) from NASA's Global Land Data Assimilation System (GLDAS version 1.0) at 1° × 1° grids for the period of August 2002 to July 2016 to estimate (equation 1) groundwater storage changes (ΔGWS) in the 37 WHYMAP large aquifer systems. This approach is consistent with previous global (Thomas et al., 2017) and basin-scale (Rodell et al., 2009; Asoka et al., 2017; Feng et al., 2018) analyses of ΔGWS from GRACE. We apply 3 gridded GRACE products (CSR, JPL-Mascons, GRGS) and an ensemble mean of ΔTWS and

individual storage component of ΔSMS and ΔSWS from 4 Land Surface Models (LSMs: CLM, Noah, VIC, Mosaic), and a single ΔSNS from Noah model (GLDAS version 2.1) to derive a total of 20 realisations of ΔGWS (Table S5) for each of the 37 aquifer systems. We then averaged all the GRACE-derived ΔGWS estimates to generate an ensemble mean ΔGWS time-series record for each aquifer system. GRACE and GLDAS LSMs derived datasets are processed and analysed in R programming language (R Core Team, 2017).

2.4 GLDAS Land Surface Models

To estimate GRACE-derived ΔGWS using equation (1), we use simulated soil moisture storage (ΔSMS), surface runoff, as a proxy for surface water storage ΔSWS (Getirana et al., 2017; Thomas et al., 2017), and snow water equivalent (ΔSNS) from NASA's Global Land Data Assimilation System (GLDAS). GLDAS system (https://ldas.gsfc.nasa.gov/gldas/) drives multiple, offline (not coupled to the atmosphere) Land Surface Models globally (Rodell et al., 2004), at variable grid resolutions (from 2.5° to 1 km), enabled by the Land Information System (LIS) (Kumar et al., 2006). Currently, GLDAS (version 1) drives four land surface models (LSMs): Mosaic, Noah, the Community Land Model (CLM), and the Variable Infiltration Capacity (VIC). We apply monthly ΔSMS (sum of all soil profiles) and ΔSWS data at a spatial resolution of 1° × 1° from 4 GLDAS LSMs: the Community Land Model (CLM, version 2.0) (Dai et al., 2003), Noah (version 2.7.1) (Ek et al., 2003), the Variable Infiltration Capacity (VIC) model (version 1.0) (Liang et al., 2003), and Mosaic (version 1.0) (Koster and Suarez, 1992). The respective total depths of modelled soil profiles are 3.4 m, 2.0 m, 1.9 m and 3.5 m in CLM (10 vertical layers), Noah (4 vertical layers), VIC (3 vertical layers), and Mosaic (3 vertical layers) (Rodell et al., 2004). For snow water equivalent (ΔSNS), we use simulated data from Noah (v.2.1) model (GLDAS version 2.1) that is forced by the global meteorological data set from Princeton University (Sheffield et

al., 2006); LSMs under GLDAS (version 1) are forced by the CPC Merged Analysis of Precipitation (CMAP) data (Rodell et al., 2004).

2.5 Global precipitation datasets

To evaluate the relationships between precipitation and GRACE-derived ΔGWS, we use a high-resolution (0.5 degree) gridded, global precipitation dataset (version 4.01) (Harris et al., 2014) available from the Climatic Research Unit (CRU) at the University of East Anglia (https://crudata.uea.ac.uk/cru/data/hrg/). In light of uncertainty in observed precipitation datasets globally, we test the robustness of relationship between precipitation and groundwater storage using the GPCC (Global Precipitation Climatology Centre) precipitation dataset (Schneider et al., 2017) (https://www.esrl.noaa.gov/psd/data/gridded/data.gpcc.html) from 1901 to 2016. Time-series (January 1901 to July 2016) of monthly precipitation from CRU and GPCC datasets for the WHYMAP aquifer systems were analysed and processed in R programming language (R Core Team, 2017).

2.6 Seasonal-Trend Decomposition (STL) of GRACE ΔGWS

Monthly time-series records (Aug 2002 to Jul 2016; supplementary Figs. S1-S36) of the ensemble mean GRACE ΔTWS and GRACE-derived ΔGWS were decomposed to seasonal, trend and remainder or residual components using a non-parametric time series decomposition technique known as "Seasonal-Trend decomposition procedure based on a locally weighted regression method called Loess (STL)" (Cleveland et al., 1990). Loess is a nonparametric method so that the fitted curve is obtained empirically without assuming the specific nature of any structure that may exist within the data (Jacoby, 2000). A key advantage of STL method is that it reveals relatively complex structures in time-series data that could easily be overlooked using traditional statistical methods such as linear regression.

192 STL decomposition technique has previously been used to analyse GRACE ΔTWS regionally
193 (Hassan and Jin, 2014) and globally (Humphrey et al., 2016). GRACE-derived ΔGWS time-
194 series records for each aquifer system were decomposed using the STL method (see equation
195 2) in the R programming language (R Core Team, 2017) as:

196 $$Y_t = T_t + S_t + R_t \quad (2)$$

197 where Y_t is the monthly ΔGWS at time t, T_t is the trend component; S_t is the seasonal
198 component; and R_t is a remainder (residual or irregular) component.

199 The STL method consists of a series of smoothing operations with different moving window
200 widths chosen to extract different frequencies within a time series, and can be regarded as an
201 extension of classical methods for decomposing a series into its individual components
202 (Chatfield, 2003). The nonparametric nature of the STL decomposition technique enables
203 detection of nonlinear patterns in long-term trends that cannot be assessed through linear
204 trend analyses (Shamsudduha et al., 2009). For STL decomposition, it is necessary to choose
205 values of smoothing parameters to extract trend and seasonal components. Selection of
206 parameters in STL decomposition is a subjective process. The choice of the seasonal
207 smoothing parameter determines the extent to which the extracted seasonal component varies
208 from year to year: a large value will lead to similar components in all years whereas a small
209 value will allow the extracted component to track the observations more closely. Similar
210 comments apply to the choice of smoothing parameter for the trend component. We
211 experimented with several different choices of smoothing parameters (see supplementary Fig.
212 S37) and checked the residuals (i.e. remainder component) for the overall performance of the
213 STL decomposition model. We conducted the Shapiro-Wilk normality test on the residuals
214 after fitting the STL smooth line with a range of trend-cycle (*t.window*) and seasonal
215 (*s.window*) windows and compared the *p* values. Visualization of the results with several

smoothing parameters (supplementary Fig. S37) and the corresponding smaller *p* values (i.e., *p* value <0.01) of the normality test suggested that the overall structure of time series at all sites could be captured reasonably well using window widths of 13 for the seasonal component and 37 for the trend. We apply the STL decomposition with a robust fitting of the loess smoother (Cleveland et al., 1990) to ensure that the fitting of the curvilinear trend does not have an adverse effect due to extreme outliers in the time-series data (Jacoby, 2000). Finally, to make the interpretation and comparison of nonlinear trends across all 37 aquifer systems, smoothing parameters were then fixed for all subsequent STL analyses.

3 Results

3.1 Variability in ΔTWS of the large aquifer systems

Ensemble mean time series of GRACE ΔTWS for the world's 37 large aquifer systems are shown in Fig. 2 (High Plains Aquifer System, no. 17) and supplementary Figs. S1-S36 (remaining 36 aquifer systems). The STL decomposition of an ensemble GRACE ΔTWS in the High Plains Aquifer System (no. 17) decomposes the time series into seasonal, trend and residual components (see supplementary Fig. S37). Variance (square of the standard deviation) in monthly GRACE ΔTWS (Figs. 3a and 4, Supplementary Table S1) is highest (>100 cm^2) primarily under monsoonal precipitation regimes within the Inter-Tropical Convergence Zone (e.g. Upper Kalahari-Cuvelai-Zambezi-11, Amazon-19, Maranho-20, Ganges-Brahmaputra-24). The sum of individual components derived from the STL decomposition (i.e., seasonal, trend and irregular or residual) approximates the overall variance in time-series data. The majority of the variance (>50%) in ΔTWS is explained by seasonality (Fig. 3a); non-linear (curvilinear) trends represent <25% of the variance in ΔTWS with the exception of the Upper Kalahari-Cuvelai-Zambezi-11 (42%). In contrast, variance in

GRACE ΔTWS in most hyper-arid and arid basins is low (Fig. 3a), <10 cm^2 (e.g., Nubian-1, NW Sahara-2, Murzuk-Djado-3, Taodeni-Tanezrouft-4, Ogaden-Juba-9, Lower Kalahari-Stampriet-12, Karoo-13, Tarim-31) and largely (> 65%) attributed to ΔGWS (Supplementary Table S2). Overall, changes in ΔTWS (i.e., difference between two consecutive hydrological years) are correlated (Pearson correlation, r >0.5, p value <0.01) to annual precipitation for 25 of the 37 large aquifer systems (Table S1). GRACE ΔTWS in aquifer systems under monsoonal precipitation regimes is strongly correlated to rainfall with a lag of 2 months (r >0.65, p value <0.01).

3.2 GRACE-ΔGWS and evidence from in-situ piezometry

Evaluations of computed GRACE-derived ΔGWS using in situ observations are limited spatially and temporally by the availability of piezometric records (Swenson et al., 2006; Strassberg et al., 2009; Scanlon et al., 2012b; Shamsudduha et al., 2012; Panda and Wahr, 2015; Feng et al., 2018). Consequently, comparisons of GRACE and in situ ΔGWS remain opportunity-driven and, here, comprise the Limpopo Basin in South Africa and Bengal Basin in Bangladesh where we possess time series records of adequate duration and density. The Bengal Basin is a part of the Ganges-Brahmaputra aquifer system (aquifer no. 24) whereas the Limpopo Basin is located between the Lower Kalahari-Stampriet Basin (aquifer no. 12) and the Karoo Basin (aquifer no. 13). The two basins feature contrasting climates (i.e. tropical humid versus tropical semi-arid) and geologies (i.e. unconsolidated sands versus weathered crystalline rock) that represent key controls on the magnitude and variability expected in ΔGWS. Both basins are in the tropics and, as such, serve less well to test the computation of GRACE-derived ΔGWS at mid and high latitudes.

In the Bengal Basin, computed GRACE and in situ ΔGWS demonstrate an exceptionally strong seasonal signal associated with monsoonal recharge that is amplified by dry-season

abstraction (Shamsudduha et al., 2009; Shamsudduha et al., 2012) and high storage of the regional unconsolidated sand aquifer, represented by a bulk specific yield (S_y) of 10% (Fig. S38a). Time-series of GRACE and LSMs are shown in Fig. S39. The ensemble mean time series of computed GRACE ΔGWS from three GRACE TWS solutions and five NASA GLDAS LSMs is strongly correlated (r = 0.86, p value <0.001) to in situ ΔGWS derived from a network of 236 piezometers (mean density of 1 piezometer per 610 km^2) for the period of 2003 to 2014. In the semi-arid Limpopo Basin where mean annual rainfall (469 mm for the period of 2003 to 2015) is one-fifth of that in the Bengal Basin (2,276 mm), the seasonal signal in ΔGWS, primarily in weathered crystalline rocks with a bulk S_y of 2.5%, is smaller (Fig. S38b). Time-series of GRACE and LSMs are shown in Fig. S40. Comparison of in situ ΔGWS, derived from a network of 40 piezometers (mean density of 1 piezometer per 1,175 km^2), and computed GRACE-derived ΔGWS shows broad correspondence (r = 0.62, p value <0.001) though GRACE-derived ΔGWS is 'noisier'; intra-annual variability may result from uncertainty in the representation of other terrestrial stores using LSMs that are used to compute GRACE-derived ΔGWS from GRACE ΔTWS. The magnitude of uncertainty in monthly ΔSWS, ΔSMS, and ΔSNS that are estimated by GLDAS LSMs to compute GRACE-derived ΔGWS in each large-scale aquifer system, is depicted in Fig. 2 and supplementary Figs. S1-S36. The favourable, statistically significant correlations between the computed ensemble mean GRACE-derived ΔGWS and in situ ΔGWS shown in these two contrasting basins indicate that, at large scales (~200,000 km^2), the methodology used to compute GRACE-derived ΔGWS has merit.

3.3 Trends in GRACE-ΔGWS time series

Computation of GRACE-derived ΔGWS for the 37 large-scale aquifers globally is shown in Figs. 2 and 5. Figure 2 shows the ensemble GRACE ΔTWS and GLDAS LSM datasets used

288 to compute GRACE-derived ΔGWS for the High Plains Aquifer System in the USA (aquifer
289 no. 17 in Fig. 1); datasets used for all other large-scale aquifer systems are given in the
290 Supplementary Material (Figs. S1–S36). In addition to the ensemble mean, we show
291 uncertainty in GRACE-derived ΔGWS associated with 20 realisations from GRACE products
292 and LSMs. Monthly time-series data of ensemble GRACE-derived ΔGWS for the other 36
293 large-scale aquifers are plotted (absolute scale) in Fig. 5 (in black) and fitted with a Loess-
294 based trend (in blue). For all but five large aquifer systems (e.g., Lake Chad Basin-
295 WHYMAP no. 7, Umm Ruwaba-8, Amazon-19, West Siberian Basin-25, and East European-
296 33), the dominant time-series component explaining variance in GRACE-derived ΔGWS is
297 trend (Fig. 3b, and supplementary Figs. S41-S77). Trends in GRACE-derived ΔGWS are,
298 however, overwhelmingly non-linear (curvilinear); linear trends adequately (R^2 >0.5, p value
299 <0.05) explain variability in GRACE-derived ΔGWS in just 5 of 37 large-scale aquifer
300 systems and of these, only two (Arabian-22, Canning-37) are declining. GRACE-derived
301 ΔGWS for three intensively developed, large-scale aquifer systems (Supplementary Table S1:
302 California Central Valley-16, Ganges-Brahmaputra-24, North China Plains-29) show
303 episodic declines (Fig. 5) though, in each case, their overall trend from 2002 to 2016 is
304 declining but non-linear (Fig. 1).

305 **3.4 Computational uncertainty in GRACE-ΔGWS**

306 For several large aquifer systems primarily in arid and semi-arid environments, we identify
307 anomalously negative or positive estimates of GRACE-derived ΔGWS that deviate
308 substantially from underlying trends (Fig. 6 and supplementary Fig. S78). For example, the
309 semi-arid Upper Kalahari-Cuvelai-Zambezi Basin (11) features an extreme, negative anomaly
310 in GRACE-derived ΔGWS (Fig. 6a) in 2007-08 that is the consequence of simulated values
311 of terrestrial stores (ΔSWS + ΔSMS) by GLDAS LSMs that exceed the ensemble GRACE
312 ΔTWS signal. Inspection of individual time-series data for this basin (Fig. S11) reveals

greater consistency in the three GRACE-ΔTWS time-series data (variance of CSR: 111 cm^2; Mascons: 164 cm^2; GRGS: 169 cm^2) compared to simulated ΔSMS among the 4 GLDAS LSMs (variance of CLM: 9 cm^2; Mosaic: 90 cm^2; Noah: 98 cm^2; VIC is 110 cm^2). In the humid Congo Basin (10), positive ΔTWS values in 2006-07 but negative ΔSMS values produce anomalously high values of GRACE-derived ΔGWS (Fig. 6b, Fig. S10). In the snow-dominated, humid Angara-Lena Basin (27), a strongly positive, combined signal of ΔSNS + ΔSWS exceeding ΔTWS leads to a very negative estimation of ΔGWS when groundwater is following a rising trend (Fig. 6c, Fig. S26).

3.5 GRACE ΔGWS and extreme precipitation

Non-linear trends in GRACE-derived ΔGWS (i.e., difference in STL trend component between two consecutive years) demonstrate a significant association with precipitation anomalies from CRU dataset for each hydrological year (i.e., percent deviations from mean annual precipitation between 2002 and 2016) in semi-arid environments (Fig. 7, Pearson correlation, $r = 0.62$, $p < 0.001$). These associations over extreme hydrological years are particularly strong in a number of individual aquifer systems (Fig. 5; Supplementary Tables S3 and S4) including the Great Artesian Basin (36) ($r = 0.93$), California Central Valley (16) ($r = 0.88$), North Caucasus Basin (34) ($r = 0.65$), Umm Ruwaba Basin (8) ($r = 0.64$), and Ogalalla (High Plains) Aquifer (17) ($r = 0.64$). In arid aquifer systems, overall associations between GRACE ΔGWS and precipitation anomalies are statistically significant but moderate ($r = 0.36$, $p < 0.001$); a strong association is found only for the Canning Basin (37) ($r = 0.52$). In humid (and sub-humid) aquifer systems, no overall statistically significant association is found yet strong correlations are noted for two temperate aquifer systems (Northern Great Plains Aquifer (14), $r = 0.51$; Angara−Lena Basin (27), $r = 0.54$); weak correlations are observed in the humid tropics for the Maranhao Basin (20, $r = 0.24$) and Ganges-Brahmaputra Basin (24, $r = 0.28$).

Distinct rises observed in GRACE-derived ΔGWS correspond with extreme seasonal (annual) precipitation (Fig. 5; Table S3 and Table S4). In the semi-arid Great Artesian Basin (aquifer no. 36) (Fig. 5 and supplementary Fig. S35), two consecutive years (2009–10 and 2010–11) of statistically extreme (i.e., >90th percentile, period: 1901 to 2016) monthly precipitation interrupt a multi-annual (2002 to 2009) declining trend. Pronounced rises in GRACE-derived ΔGWS in response to extreme annual rainfall are visible in other semi-arid, large aquifer systems including the Umm Ruwaba Basin (8) in 2007, Lower Kalahari-Stampriet Basin (12) in 2011, California Central Valley (16) in 2005, Ogalalla (High Plains) Aquifer (17) in 2015, and Indus Basin (23) in 2010 and 2015 (Tables S3 and S4 and Figs. S2, S8, S12, S16, S22). Similar rises in GRACE-derived ΔGWS in response to extreme annual rainfall in arid basins include the Lake Chad Basin (7) in 2012 and Ogaden-Juba Basin (9) in 2013 (Table S3 and Figs. S7, S9). In the Canning Basin, a substantial rise in GRACE-derived ΔGWS occurs in 2010–11 (Tables S3 and S4 and Fig. S36) in response to extreme annual rainfall though the overall trend is declining.

Non-linear trends that feature substantial rises in GRACE-derived ΔGWS in response to extreme annual precipitation under humid climates, are observed in the Maranhao Basin (20) in 2008-09, Guarani Aquifer System (21) in 2015-16, and North China Plains (29) in 2003. Consecutive years of extreme precipitation in 2012 and 2013 also generate a distinct rise in GRACE-derived ΔGWS in the Song-Liao Plain (30) (Tables S3 and S4 and Figs. S29). In the heavily developed (Table S2) Ganges-Brahmaputra Basin (24), a multi-annual (2002 to 2010) declining trend is halted by an extreme (i.e., highest over the GRACE period of 2002 to 2016 but 59th percentile over the period of 1901 to 2016 using CRU dataset) annual precipitation in 2011 (Tables S3 and S4 and Figs. S23). Consecutive years from 2014 to 2015 of extreme annual precipitation increase GRACE-derived ΔGWS and disrupt a multi-annual declining trend in the West Siberian Artesian Basin (25) (Tables S3 and S4 and Figs. S24). In the sub-

363 humid Northern Great Plains (14), distinct rises in GRACE-derived ΔGWS occur in 2010
364 (Tables S3 and S4 and Figs. S14) in response to extreme annual precipitation though the
365 overall trend is linear and rising. The overall agreement in mean annual precipitation between
366 the CRU and GPCC datasets for the period of 1901 to 2016 is strong (median correlation
367 coefficient in 37 aquifer systems, $r = 0.92$).

368

369 # 4 Discussion

370 ## 4.1 Uncertainty in GRACE-derived ΔGWS

371 We compute the range of uncertainty in GRACE-derived ΔGWS associated with 20 potential
372 realisations from applied GRACE (CSR, JPL-Mascons, GRGS) products and LSMs (CLM,
373 Noah, VIC, Mosaic). Uncertainty is generally higher for aquifers systems located in arid to
374 hyper-arid environments (Table 2, see supplementary Fig. S79). Computation of GRACE-
375 derived ΔGWS relies upon uncalibrated simulations of individual terrestrial water stores (i.e.,
376 ΔSWS, ΔSWS, ΔSNS) from LSMs to estimate ΔGWS from GRACE ΔTWS. A recent
377 global-scale comparison of ΔTWS estimated by GLDAS LSMs and GRACE (Scanlon et al.,
378 2018) indicates that LSMs systematically underestimate water storage changes. Further, the
379 absence of river-routing and representation of lakes and reservoirs in the estimation of ΔSWS
380 by LSMs constrains computation of GRACE ΔGWS as similarly recognised by Scanlon et al.
381 (2019). Finally, substantial variability in ΔSMS among GLDAS models and the limited depth
382 (<3.5 m below ground level) to the deepest soil layer over which these LSMs simulate ΔSMS
383 also hamper estimation of GRACE ΔGWS, especially in drylands where the thickness of
384 unsaturated zones may an order of magnitude greater (Scanlon et al., 2009).

385 We detect probable errors in GLDAS LSM data from events that produce large deviations in
386 GWS (Fig. 5). These errors occur because GRACE-derived ΔGWS is computed as residual

(equation 1); overestimation (or underestimation) of these combined stores produces negative (or positive) values of GRACE-derived ΔGWS when the aggregated value of other terrestrial water stores is strongly positive (or negative) and no lag is assumed (Shamsudduha et al., 2017). Evidence from limited piezometric data presented here and elsewhere (Panda and Wahr, 2015; Feng et al., 2018) suggests that the dynamics in computed GRACE-derived ΔGWS are nonetheless reasonable yet the amplitude in ΔGWS from piezometry is scalable due to uncertainty in the applied S_y (Shamsudduha et al., 2012).

Assessments of ΔGWS derived from GRACE are constrained by both their limited timespan (2002–2016) and course spatial resolution (>200,000 km^2). For example, centennial-scale piezometry in the Ganges-Brahmaputra aquifer system (no. 24) reveals that recent groundwater depletion, (i.e., groundwater withdrawals that are unlikely to be replenished within a century as per Bierkens and Wada (2019)), in NW India traced by GRACE (Fig. 5 and supplementary Fig. S23) (Rodell et al., 2009; Chen et al., 2014) follows more than a century of groundwater accumulation (see supplementary Fig. S80) through leakage of surface water via a canal network constructed primarily during the 19th century (MacDonald et al., 2016). Long-term piezometric records from central Tanzania and the Limpopo Basin of South Africa (Supplementary Fig. S81) show dramatic increases in ΔGWS associated with extreme seasonal rainfall events that occurred prior to 2002 and thus provide a vital context to the more recent period of ΔGWS estimated by GRACE. At regional scales, GRACE-derived ΔGWS can differ substantially from more localised, in situ observations of ΔGWS from piezometry. In the Karoo Basin (aquifer no. 13), GRACE-derived ΔGWS is also rising (Fig. 5 and supplementary Fig. S13) over periods during which groundwater depletion has been reported in parts of the basin (Rosewarne et al., 2013). In the Guarani Aquifer System (21), groundwater depletion is reported from 2005 to 2009 in Ribeiro Preto near Sao Paulo as

411 a result of intensive groundwater withdrawals for urban water supplies and irrigation of
412 sugarcane (Foster et al., 2009) yet GRACE-derived ΔGWS over this same period is rising.

413 **4.2 Variability in GRACE ΔGWS and role of extreme precipitation**

414 Non-linear trends in GRACE-derived ΔGWS arise, in part, from inter-annual variability in
415 precipitation which has similarly been observed in analyses of GRACE ΔTWS (Humphrey et
416 al., 2016; Sun et al., 2017; Bonsor et al., 2018). Annual precipitation in the Great Artesian
417 Basin (aquifer no. 36) provides a dramatic example of how years (2009–10, 2010–11 from
418 both CRU and GPCC datasets) of extreme precipitation can generate anomalously high
419 groundwater recharge that arrests a multi-annual declining trend (Fig. 5), increasing
420 variability in GRACE-derived ΔGWS over the relatively short period (15 years) of GRACE
421 data. The disproportionate contribution of episodic, extreme rainfall to groundwater recharge
422 has previously been shown by (Taylor et al., 2013b) from long-term piezometry in semi-arid
423 central Tanzania where nearly 20% of the recharge observed over a 55-year period resulted
424 from a single season of extreme rainfall, associated with the strongest El Niño event (1997–
425 1998) of the last century (Supplementary Fig. S81a). Further analysis from multi-decadal
426 piezometric records in drylands across tropical Africa (Cuthbert et al., 2019) confirm this bias
427 in response to intensive precipitation.

428 The dependence of groundwater replenishment on extreme annual precipitation indicated by
429 GRACE-derived ΔGWS for many of the world's large aquifer systems is consistent with
430 evidence from other sources. In a pan-tropical comparison of stable-isotope ratios of oxygen
431 (^{18}O:^{16}O) and hydrogen (^{2}H:^{1}H) in rainfall and groundwater, Jasechko and Taylor (2015)
432 show that recharge is biased to intensive monthly rainfall, commonly exceeding the 70th
433 percentile. In humid Uganda, Owor et al. (2009) demonstrate that groundwater recharge
434 observed from piezometry is more strongly correlated to daily rainfall exceeding a threshold

435 (10 mm) than all daily rainfalls. Periodicity in groundwater storage indicated by both
436 GRACE and in situ data has been associated with large-scale synoptic controls on
437 precipitation (e.g., El Niño Southern Oscillation, Pacific Decadal Oscillation,) in southern
438 Africa (Kolusu et al., 2019), and have been shown to amplify recharge in major US aquifers
439 (Kuss and Gurdak, 2014) and groundwater depletion in India (Mishra et al., 2016).

440 In some large-scale aquifer systems, GRACE-derived ΔGWS exhibits comparatively weak
441 correlations to precipitation. In the semi-arid Iullemmeden-Irhazer Aquifer (6) variance in
442 rainfall over the period of GRACE observation following the multi-decadal Sahelian drought
443 is low (Table S1) and the net rise in GRACE-derived ΔGWS is associated with changes in
444 the terrestrial water balance resulting from land-cover change (Ibrahim et al., 2014). In the
445 Amazon (16), rising trends in GRACE-derived ΔGWS, which are aligned to ΔTWS reported
446 previously by Scanlon et al. (2018) and Rodell et al. (2018), occur during a period (2010–
447 2016; see supplementary Table S18) that is the driest since the 1980s (Chaudhari et al.,
448 2019); analyses over the longer term (1980–2015) point nevertheless to an overall
449 intensification of the Amazonian hydrological cycle.

450 **4.3 Trends in GRACE ΔGWS under global change**

451 Our analysis identifies non-linear trends in GRACE-derived ΔGWS for the vast majority (32
452 of 37) of the world's large aquifer systems (Figs. 1, 5 and 8). Non-linearity reflects, in part,
453 the variable nature of groundwater replenishment observed at the scale of the GRACE
454 footprint that is consistent with more localised, emerging evidence from multi-decadal
455 piezometric records (Taylor et al., 2013b) (Supplementary Fig. S81a). The variable and often
456 episodic nature of groundwater replenishment complicates assessments of the sustainability
457 of groundwater withdrawals and highlights the importance of long-term observations over
458 decadal timescales in undertaking such evaluations. Dramatic rises in freshwater withdrawals,

459 primarily associated with the expansion of irrigated agriculture in semi-arid environments,
460 have nevertheless led to groundwater depletion, computed globally from hydrological models
461 (e.g., Wada et al., 2010; de Graaf et al., 2017) and volumetric-based calculations (Konikow,
462 2011). Further, groundwater depletion globally has been shown to contribute to sea-level rise
463 (e.g., Wada et al., 2016). However, as recognised in a comprehensive review by Bierkens
464 and Wada (2019), groundwater depletion is often localised, occurring below the footprint
465 (200,000 km^2) of GRACE as has been well demonstrated by detailed modelling studies in the
466 California Central Valley (Scanlon et al., 2012a) and North China Plain (Cao et al., 2013).

467 Projections of the sustainability of groundwater withdrawals under global change are
468 complicated, in part, by uncertainty in how radiative forcing will affect large-scale, regional
469 controls on extreme annual precipitation like El Niño Southern Oscillation (Latif and
470 Keenlyside, 2009). Globally, Reager et al. (2016) show a trend towards enhanced
471 precipitation on the land under climate change. Given this trend and the observed
472 intensification of precipitation on land from global warming (Allan et al., 2010; Westra et al.,
473 2013; Zhang et al., 2013; Myhre et al., 2019), groundwater recharge to many large-scale
474 aquifer systems may increase under climate change as revealed by the statistical relationships
475 found in this study between ΔGWS and extreme annual precipitation. The magnitude of this
476 increase is, however, unlikely to offset the impact of human withdrawals in areas of intensive
477 abstraction for irrigated agriculture as shown in NW India by Xie et al. (2020). The
478 developed set of GRACE-derived ΔGWS time series data for the world's large aquifer
479 systems provided here offers a consistent, additional benchmark alongside long-term
480 piezometry to assess not only large-scale climate controls on groundwater replenishment but
481 also opportunities to enhance groundwater storage through managed aquifer recharge.

482

5 Conclusions

Changes in groundwater storage (ΔGWS) computed from GRACE satellite data continue to rely upon uncertain, uncalibrated estimates of changes in other terrestrial stores of water found in soil, surface water, and snow/ice from global-scale models. The application here of ensemble mean values of three GRACE ΔTWS processing strategies (CSR, JPL-Mascons, GRGS) and five land-surface models (GLDAS 1: CLM, Noah, VIC, Mosaic; GLDAS 2: Noah) is designed to reduce the impact of uncertainty in an individual model or GRACE product on the computation of GRACE-derived ΔGWS. We, nevertheless, identify a few instances where erroneously high or low values of GRACE-derived ΔGWS are computed; these occur primarily in arid and semi-arid environments where uncertainty in the simulation of terrestrial water balances is greatest. Over the period of GRACE observation (2002 to 2016), we show favourable comparisons between GRACE-derived ΔGWS and piezometric observations (r = 0.62 to 0.86) in two contrasting basins (i.e., semi-arid Limpopo Basin, tropical humid Bengal Basin) for which in situ data are available. This study thus contributes to a growing body of research and observations reconciling computed GRACE-derived ΔGWS to ground-based data.

GRACE-derived ΔGWS from 2002 to 2016 for the world's 37 large-scale aquifer systems shows substantial variability as revealed explicitly by 20 potential realisations from GRACE products and LSMs computed here; trends in ensemble mean GRACE-derived ΔGWS are overwhelmingly (87%) non-linear. Linear trends adequately explain variability in GRACE-derived ΔGWS in just 5 aquifer systems for which linear declining trends, indicative of groundwater depletion, are observed in 2 aquifer systems (Arabian, Canning); overall trends for three intensively developed, large-scale aquifer systems (California Central Valley, Ganges-Brahmaputra, North China Plains) are declining but non-linear. This non-linearity in GRACE-derived ΔGWS for the vast majority of the world's large aquifer systems is

inconsistent with previous analyses at the scale of GRACE footprint (~200,000 km^2) asserting global-scale groundwater depletion. Groundwater depletion, more commonly observed by piezometry, is experienced at scales well below the GRACE footprint and is likely to be more pervasive than suggested by the presented analysis of large-scale aquifers. Non-linearity in GRACE-derived ΔGWS arises, in part, from episodic recharge associated with extreme (>90^{th} percentile) annual precipitation. This episodic replenishment of groundwater, combined with natural discharges that sustain ecosystem functions and human withdrawals, produces highly dynamic aquifer systems that complicate assessments of the sustainability of groundwater withdrawals from large aquifer systems. These findings highlight, however, potential opportunities for sustaining groundwater withdrawals through induced recharge from extreme precipitation and managed aquifer recharge.

519 **References**

520 Allan, R. P., Soden, B. J., John, V. O., Ingram, W., and Good, P.: Current changes in tropical
521 precipitation, Environmental Research Letters, 5, 025205, 10.1088/1748-
522 9326/5/2/025205, 2010.

523 Asoka, A., Gleeson, T., Wada, Y., and Mishra, V.: Relative contribution of monsoon
524 precipitation and pumping to changes in groundwater storage in India, Nature
525 Geoscience, 10, 109-117, 2017.

526 Bhanja, S. N., Mukherjee, A., Saha, D., Velicogna, I., and Famiglietti, J. S.: Validation of
527 GRACE based groundwater storage anomaly using in-situ groundwater level
528 measurements in India, Journal of Hydrology, 543, 729-738, 2016.

529 Biancale, R., Lemoine, J.-M., Balmino, G., Loyer, S., Bruisma, S., Perosanz, F., Marty, J.-C.,
530 and Gégout, P.: 3 Years of Geoid Variations from GRACE and LAGEOS Data at 10-day
531 Intervals from July 2002 to March 2005, CNES/GRGS, 2006.

532 Bierkens, M. F. P., and Wada, Y.: Non-renewable groundwater use and groundwater
533 depletion: a review, Environ. Res. Lett., 14, 063002, 10.1088/1748-9326/ab1a5f, 2019.

534 Bonsor, H. C., Shamsudduha, M., Marchant, B. P., MacDonald, A. M., and Taylor, R. G.:
535 Seasonal and Decadal Groundwater Changes in African Sedimentary Aquifers Estimated
536 Using GRACE Products and LSMs, Remote Sensing, 10, 2018.

537 Cao, G., Zheng, C., Scanlon, B. R., Liu, J., and Li, W.: Use of flow modeling to assess
538 sustainability of groundwaterresources in the North China Plain, Water Resour. Res., 49,
539 10.1029/2012WR011899, 2013.

540 Castellazzi, P., Martel, R., Rivera, A., Huang, J., Pavlic, G., Calderhead, A. I., Chaussard, E.,
541 Garfias, J., and Salas, J.: Groundwater depletion in Central Mexico: Use of GRACE and
542 InSAR to support water resources management, Water Resour. Res., 52, 5985-6003,
543 doi:10.1002/2015WR018211, 2016.

544 Chatfield, C.: The analysis of time series - an introduction, 6th ed., Chapman and Hall, CRC
545 Press, Boca Raton, 2003.

546 Chaudhari, S., Pokhrel, Y., Moran, E., and Miguez-Macho, G.: Multi-decadal hydrologic
547 change and variability in the Amazon River basin: understanding terrestrial water storage
548 variations and drought characteristics, Hydrol. Earth Syst. Sci., 23, 2841–2862,
549 10.5194/hess-23-2841-2019, 2019.

550 Chen, J., Li, J., Zhang, Z., and Ni, S.: Long-term groundwater variations in Northwest India
551 from satellite gravity measurements, Global and Planetary Change, 116, 130-138, 2014.

552 Cleveland, R. B., Cleveland, W. S., McRae, J. E., and Terpenning, I.: STL: A Seasonal Trend
553 Decomposition Procedure Based on LOESS, J. Official Statistics, 6, 3-33, 1990.

554 Cuthbert, M. O., Taylor, R. G., Favreau, G., Todd, M. C., Shamsudduha, M., Villholth, K. G.,
555 MacDonald, A. M., Scanlon, B. R., Kotchoni, D. O. V., Vouillamoz, J.-M., Lawson, F.
556 M. A., Adjomayi, P. A., Kashaigili, J., Seddon, D., Sorensen, J. P. R., Ebrahim, G. Y.,
557 Owor, M., Nyenje, P. M., Nazoumou, Y., Goni, I., Ousmane, B. I., Sibanda, T., Ascott,
558 M. J., Macdonald, D. M. J., Agyekum, W., Koussoubé, Y., Wanke, H., Kim, H., Wada,
559 Y., Lo, M.-H., Oki, T., and Kukuric, N.: Observed controls on resilience of groundwater
560 to climate variability in sub-Saharan Africa, Nature, 572, 230–234,
561 https://doi.org/10.1038/s41586-019-1441-7, 2019.

562 Dai, Y., Zeng, X., Dickinson, R. E., Baker, I., Bonan, G. B., Bosilovich, M. G., Denning, A.
563 S., Dirmeyer, P. A., Houser, P. R., Niu, G., Oleson, K. W., Schlosser, C. A., and Yang,
564 Z.-L.: The common land model (CLM), Bull. Am. Meteorol. Soc., 84, 1013-1023, 2003.

565 de Graaf, I. E. M., van Beek, L. P. H., Gleeson, T., Moosdorf, N., Schmitz, O., Sutanudjaja,
566 E. H., and Bierkens, M. F. P.: A global-scale two layer transient groundwater model:
567 development and application to groundwater depletion, Adv. Water Resour., 102, 53–67,
568 2017.

569 Döll, P., Hoffmann-Dobrev, H., Portmann, F. T., Siebert, S., Eicker, A., Rodell, M.,
570 Strassberg, G., and Scanlon, B. R.: Impact of water withdrawals from groundwater and
571 surface water on continental water storage variations, Journal of Geodynamics, 59-60,
572 143-156, 2012.

573 Döll, P., Schmied, H. M., Schuh, C., Portmann, F. T., and Eicker, A.: Global-scale
574 assessment of groundwater depletion and related groundwater abstractions: Combining
575 hydrological modeling with information from well observations and GRACE satellites,
576 Water Resour. Res., 50, 5698-5720, doi:10.1002/2014WR015595, 2014.

577 Ek, M. B., Mitchell, K. E., Lin, Y., Rogers, E., Grunmann, P., Koren, V., Gayno, G., and
578 Tarpley, J. D.: Implementation of Noah land surface model advances in the National
579 Centers for Environmental Prediction operational mesoscale Eta model, J. Geophys.
580 Res., 108(D22), 8851, 10.1029/2002JD003296, 2003.

581 Famiglietti, J. S., Lo, M., Ho, S. L., Bethune, J., Anderson, K. J., Syed, T. H., Swenson, S.
582 C., Linage, C. R. d., and Rodell, M.: Satellites measure recent rates of groundwater
583 depletion in California's Central Valley, Geophys. Res. Lett., 38, L03403,
584 10.1029/2010GL046442, 2011.

585 Famiglietti, J. S., and Rodell, M.: Water in the Balance, Science, 340, 1300-1301,
586 doi:10.1126/science.1236460, 2013.

587 Famiglietti, J. S.: The global groundwater crisis, Nature Climate Change, 4, 945-948,
588 doi:10.1038/nclimate2425, 2014.

589 Feng, W., Shum, C. K., Zhong, M., and Pan, Y.: Groundwater Storage Changes in China
590 from Satellite Gravity: An Overview, Remote Sensing, 10, 674, 2018.

591 Foster, S., Hirata, R., Vidal, A., Schmidt, G., and Garduño, H.: The Guarani Aquifer
592 Initiative - Towards Realistic Groundwater Management in a Transboundary Context,
593 The World Bank, Washington D.C., 28, 2009.

594 Getirana, A., Kumar, S., Girotto, M., and Rodell, M.: Rivers and Floodplains as Key
595 Components of Global Terrestrial Water Storage Variability, Geophysical Research
596 Letters, 44, 10359-10368, 2017.

597 Hanasaki, N., Yoshikawa, S., Pokhrel, Y., and Kanae, S.: A global hydrological simulation to
598 specify the sources of water used by humans, Hydrol. Earth Syst. Sci., 22, 789-817,
599 10.5194/hess-22-789-2018, 2018.

600 Harris, I., Jones, P. D., Osborn, T. J., and Lister, D. H.: Updated high-resolution grids of
601 monthly climatic observations - the CRU TS3.10 Dataset, International Journal of
602 Climatology, 34, 623-642, 2014.

603 Hassan, A. A., and Jin, S.: Lake level change and total water discharge in East Africa Rift
604 Valley from satellite-based observations, Global Planet Change, 117, 79-90,
605 10.1016/j.gloplacha.2014.03.005, 2014.

606 Humphrey, V., Gudmundsson, L., and Seneviratne, S. I.: Assessing Global Water Storage
607 Variability from GRACE: Trends, Seasonal Cycle, Subseasonal Anomalies and
608 Extremes, Surveys in Geophysics, 37, 357-395, doi:10.1007/s10712-016-9367-1, 2016.

609 Ibrahim, M., Favreau, G., Scanlon, B. R., Seidel, J. L., Coz, M. L., Demarty, J., and
610 Cappelaere, B.: Long-term increase in diffuse groundwater recharge following expansion
611 of rainfed cultivation in the Sahel, West Africa, Hydrogeology Journal, 22, 1293-1305,
612 2014.

613 Jacoby, W. G.: Loess::a nonparametric, graphical tool for depicting relationships between
614 variables, Electoral Studies, 19, 577-613, 2000.

615 Jasechko, S., and Taylor, R. G.: Intensive rainfall recharges tropical groundwaters,
616 Environmental Research Letters, 10, 124015, 2015.

617 Kim, H., Yeh, P. J.-F., Oki, T., and Kanae, S.: Role of rivers in the seasonal variations of
618 terrestrial water storage over global basins, Geophys. Res. Lett., 36, L17402,
619 doi:10.1029/2009GL039006, 2009.

620 Kolusu, S. R., Shamsudduha, M., Todd, M. C., Taylor, R. G., Seddon, D., Kashaigili, J. J.,
621 Girma, E., Cuthbert, M., Sorensen, J. P. R., Villholth, K. G., MacDonald, A. M., and
622 MacLeod, D. A.: The El Niño event of 2015-16: Climate anomalies and their impact on
623 groundwater resources in East and Southern Africa, Hydrol. Earth Syst. Sci., 23, 1751-
624 1762, 2019.

625 Konikow, L. F.: Contribution of global groundwater depletion since 1900 to sea-level rise,
626 Geophys. Res. Lett. , 38, L17401, 10.1029/2011GL048604, 2011.

627 Koster, R. D., and Suarez, M. J.: Modeling the land surface boundary in climate models as a
628 composite of independent vegetation stands, J. Geophys. Res., 97, 2697-2715, 1992.

629 Kumar, S. V., Peters-Lidard, C. D., Tian, Y., Houser, P. R., Geiger, J., Olden, S., Lighty, L.,
630 Eastman, J. L., Doty, B., Dirmeyer, P., Adams, J., Mitchell, K., Wood, E. F., and
631 Sheffield, J.: Land information system: An interoperable framework for high resolution
632 land surface modeling, Environmental Modelling & Software, 21, 1402-1415, 2006.

633 Kuss, A. J. M., and Gurdak, J. J.: Groundwater level response in U.S. principal aquifers to
634 ENSO, NAO, PDO, and AMO, Journal of Hydrology, 519 (Part B), 1939-1952, 2014.

635 Landerer, F. W., and Swenson, S. C.: Accuracy of scaled GRACE terrestrial water storage
636 estimates, Water Resour. Res., 48, W04531, 2012.

637 Latif, M., and Keenlyside, N. S.: El Niño/Southern Oscillation response to global warming,
638 Proceedings of the National Academy of Sciences, 106, 20578-20583,
639 doi:10.1073/pnas.0710860105, 2009.

640 Liang, X., Xie, Z., and Huang, M.: A new parameterization for surface and groundwater
641 interactions and its impact on water budgets with the variable infiltration capacity (VIC)
642 land surface model, J. Geophys. Res., 108(D16), 8613, 10.1029/2002JD003090, 2003.

643 Longuevergne, L., Wilson, C. R., Scanlon, B. R., and Crétaux, J. F.: GRACE water storage
644 estimates for the Middle East and other regions with significant reservoir and lake
645 storage, Hydrol. Earth Syst. Sci., 17, 4817-4830, doi:10.5194/hess-17-4817-2013, 2013.

646 MacDonald, A. M., Bonsor, H. C., Ahmed, K. M., Burgess, W. G., Basharat, M., Calow, R.
647 C., Dixit, A., Foster, S. S. D., Gopal, K., Lapworth, D. J., Lark, R. M., Moench, M.,
648 Mukherjee, A., Rao, M. S., Shamsudduha, M., Smith, L., Taylor, R. G., Tucker, J., van

Steenbergen, F., and Yadav, S. K.: Groundwater quality and depletion in the Indo-Gangetic Basin mapped from in situ observations, Nature Geoscience, 9, 762-766, 2016.

Mishra, V., Aadhar, S., Asoka, A., S. Pai, and Kumar, R.: On the frequency of the 2015 monsoon season drought in the Indo-Gangetic Plain, Geophys. Res. Lett., 43, 12102–12112, 10.1002/GL071407, 2016.

Myhre, G., Alterskjær, K., Stjern, C. W., Hodnebrog, Ø., Marelle, L., Samset, B. H., Sillmann, J., Schaller, N., Fischer, E., Schulz, M., and Stohl, A.: Frequency of extreme precipitation increases extensively with event rareness under global warming, Scientific Reports, 9, 16063, 10.1038/s41598-019-52277-4, 2019.

Owor, M., Taylor, R. G., Tindimugaya, C., and Mwesigwa, D.: Rainfall intensity and groundwater recharge: empirical evidence from the Upper Nile Basin, Environmental Research Letters, 1-6, 2009.

Panda, D. K., and Wahr, J.: Spatiotemporal evolution of water storage changes in India from the updated GRACE-derived gravity records, Water Resour. Res., 51, 135–149, doi:10.1002/2015WR017797, 2015.

Reager, J. T., Gardner, A. S., Famiglietti, J. S., Wiese, D. N., Eicker, A., and Lo, M.-H.: A decade of sea level rise slowed by climate-driven hydrology, Science, 351, 699-703, 2016.

Richey, A. S., Thomas, B. F., Lo, M.-H., Reager, J. T., Famiglietti, J. S., Voss, K., Swenson, S., and Rodell, M.: Quantifying renewable groundwater stress with GRACE, Water Resour. Res., 51, 5217-5238, doi:10.1002/2015WR017349, 2015.

Richts, A., Struckmeier, W. F., and Zaepke, M.: WHYMAP and the Groundwater Resources of the World 1:25,000,000, in: Sustaining Groundwater Resources. International Year of Planet Earth, edited by: J., J., Springer, Dordrecht, 159-173, 2011.

Rodell, M., Houser, P. R., Jambor, U., Gottschalck, J., Mitchell, K., Meng, C.-J., Arsenault, K., Cosgrove, B., Radakovich, J., Bosilovich, M., Entin, J. K., Walker, J. P., Lohmann, D., and Toll, D.: The Global Land Data Assimilation System, Bull. Am. Meteorol. Soc., 85, 381-394, 2004.

Rodell, M., Chen, J., Kato, H., Famiglietti, J. S., Nigro, J., and Wilson, C. R.: Estimating ground water storage changes in the Mississippi River basin (USA) using GRACE, Hydrogeology Journal, 15, 159-166, doi:10.1007/s10040-006-0103-7, 2007.

Rodell, M., Velicogna, I., and Famiglietti, J. S.: Satellite-based estimates of groundwater depletion in India, Nature, 460, 999-1003, doi:10.1038/nature08238, 2009.

Rodell, M., Famiglietti, J. S., Wiese, D. N., Reager, J. T., Beaudoing, H. K., Landerer, F. W., and Lo, M. H.: Emerging trends in global freshwater availability, Nature, 557, 651-659, 10.1038/s41586-018-0123-1, 2018.

Rosewarne, P. N., Woodford, A. C., O'Brien, R., Tonder, G. V., Esterhuyse, C., Goes, M., Talma, A. S., Tredoux, G., and Visser, D.: Karoo Groundwater Atlas, Volume 2. Karoo Groundwater Expert Group (KGEG), Ground Water Division, The Geological Society of South Africa, Cape Town, South Africa, 1-35, 2013.

Scanlon, B. R., Stonestrom, D. A., Reedy, R. C., Leaney, F. W., Gates, J., and Cresswell, R. G.: Inventories and mobilization of unsaturated zone sulfate, fluoride, and chloride related to land use change in semiarid regions, southwestern United States and Australia, Water Resour. Res., 45, W00A18, 10.1029/2008WR006963, 2009.

693 Scanlon, B. R., Faunt, C. C., Longuevergne, L., Reedy, R. C., Alley, W. M., McGuire, V. L.,
694 and McMahon, P. B.: Groundwater depletion and sustainability of irrigation in the US
695 High Plains and Central Valley, Proc. Natl. Acad. Sci. USA, 109, 9320-9325, 2012a.

696 Scanlon, B. R., Longuevergne, L., and Long, D.: Ground referencing GRACE satellite
697 estimates of groundwater storage changes in the California Central Valley, USA, Water
698 Resour. Res., 48, W04520, 2012b.

699 Scanlon, B. R., Zhang, Z., Save, H., Sun, A. Y., Müller Schmied, H., van Beek, L. P. H.,
700 Wiese, D. N., Wada, Y., Long, D., Reedy, R. C., Longuevergne, L., Döll, P., and
701 Bierkens, M. F. P.: Global models underestimate large decadal declining and rising water
702 storage trends relative to GRACE satellite data, PNAS, 115 1080-1089,
703 doi:10.1073/pnas.1704665115, 2018.

704 Scanlon, B. R., Zhang, Z., Rateb, A., Sun, A., Wiese, D., Save, H., Beaudoing, H., Lo, M. H.,
705 Müller-Schmied, H., Döll, P., van Beek, R., Swenson, S., Lawrence, D., Croteau, M.,
706 and Reedy, R. C.: Tracking seasonal fluctuations in land water storage using global
707 models and GRACE satellites, Geophysical Research Letters, 46, 5254–5264,
708 10.1029/2018GL081836, 2019.

709 Schneider, U., Finger, P., Meyer-Christoffer, A., Rustemeier, E., Ziese, M., and Becker, A.:
710 Evaluating the Hydrological Cycle over Land Using the Newly-Corrected Precipitation
711 Climatology from the Global Precipitation Climatology Centre (GPCC), Atmosphere, 8,
712 52, 10.3390/atmos8030052, 2017.

713 Shamsudduha, M., Chandler, R. E., Taylor, R. G., and Ahmed, K. M.: Recent trends in
714 groundwater levels in a highly seasonal hydrological system: the Ganges-Brahmaputra-
715 Meghna Delta, Hydrol. Earth Syst. Sci., 13, 2373-2385, doi:10.5194/hess-13-2373-2009,
716 2009.

717 Shamsudduha, M., Taylor, R. G., and Longuevergne, L.: Monitoring groundwater storage
718 changes in the highly seasonal humid tropics: validation of GRACE measurements in the
719 Bengal Basin, Water Resour. Res., 48, W02508, doi:10.1029/2011WR010993, 2012.

720 Shamsudduha, M., Taylor, R. G., Jones, D., Longuevergne, L., Owor, M., and Tindimugaya,
721 C.: Recent changes in terrestrial water storage in the Upper Nile Basin: an evaluation of
722 commonly used gridded GRACE products, Hydrol. Earth Syst. Sci., 21, 4533-4549,
723 2017.

724 Sheffield, J., Goteti, G., and Wood, E. F.: Development of a 50-year high-resolution global
725 dataset of meteorological forcings for land surface modeling, Journal of Climate, 19,
726 3088-3111, 2006.

727 Strassberg, G., Scanlon, B. R., and Chambers, D.: Evaluation of groundwater storage
728 monitoring with the GRACE satellite: Case study of the High Plains aquifer, central
729 United States, Water Resour. Res., 45, W05410, 2009.

730 Sun, A. Y., Scanlon, B. R., AghaKouchak, A., and Zhang, Z.: Using GRACE Satellite
731 Gravimetry for Assessing Large-Scale Hydrologic Extremes, Remote Sensing, 9, 1287,
732 doi:10.3390/rs9121287, 2017.

733 Swenson, S., Yeh, P. J.-F., Wahr, J., and Famiglietti, J. S.: A comparison of terrestrial water
734 storage variations from GRACE with in situ measurements from Illinois, Geophys. Res.
735 Lett., 33, L16401, doi:10.1029/2006GL026962, 2006.

Swenson, S., Famiglietti, J., Basara, J., and Wahr, J.: Estimating profile soil moisture and groundwater variations using GRACE and Oklahoma Mesonet soil moisture data, Water Resour. Res., 44, W01413, doi:10.1029/2007WR006057, 2008.

Tapley, B. D., Bettadpur, S., Ries, J. C., Thompson, P. F., and Watkins, M. M.: GRACE measurements of mass variability in the Earth system, Science, 305, 503-505, 2004.

Taylor, R. G., Scanlon, B., Doll, P., Rodell, M., van Beek, R., Wada, Y., Longuevergne, L., Leblanc, M., Famiglietti, J. S., Edmunds, M., Konikow, L., Green, T. R., Chen, J., Taniguchi, M., Bierkens, M. F. P., MacDonald, A., Fan, Y., Maxwell, R. M., Yechieli, Y., Gurdak, J. J., Allen, D. M., Shamsudduha, M., Hiscock, K., Yeh, P. J. F., Holman, I., and Treidel, H.: Ground water and climate change, Nature Climate Change, 3, 322-329, doi:10.1038/nclimate1744, 2013a.

Taylor, R. G., Todd, M. C., Kongola, L., Maurice, L., Nahozya, E., Sanga, H., and MacDonald, A.: Evidence of the dependence of groundwater resources on extreme rainfall in East Africa, Nature Climate Change, 3, 374-378, doi:10.1038/nclimate1731, 2013b.

Thomas, B. F., Caineta, J., and Nanteza, J.: Global assessment of groundwater sustainability based on storage anomalies, Geophysical Research Letters, 44, 11445-11455, doi:10.1002/2017GL076005, 2017.

Wada, Y., van Beek, L. P. H., van Kempen, C. M., Reckman, J. W. T. M., Vasak, S., and Bierkens, M. F. P.: Global depletion of groundwater resources, Geophysical Research Letters, 37, L20402, 10.1029/2010GL044571, 2010.

Wada, Y., Wisser, D., and Bierkens, M. F. P.: Global modeling of withdrawal, allocation and consumptive use of surface water and groundwater resources, Earth Syst. Dynam., 5, 15-40, 10.5194/esd-5-15-2014, 2014.

Wada, Y., Lo, M.-H., Yeh, P. J. F., Reager, J. T., Famiglietti, J. S., Wu, R.-J., and Tseng, Y.-H.: Fate of water pumped from underground and contributions to sea-level rise, Nature Climate Change, 6, 777-780, 10.1038/nclimate3001, 2016.

Watkins, M. M., Wiese, D. N., Yuan, D.-N., Boening, C., and Landerer, F. W.: Improved methods for observing Earth's time variable mass distribution with GRACE using spherical cap mascons, J. Geophys. Res. Solid Earth, 120, 2648–2671, doi:10.1002/2014JB011547, 2015.

Westra, S., Alexander, L. V., and Zwiers, F. W.: Global Increasing Trends in Annual Maximum Daily Precipitation, J. Climate, 26, 3904–3918, 10.1175/JCLI-D-12-00502.1, 2013.

Wiese, D. N., Landerer, F. W., and Watkins, M. M.: Quantifying and reducing leakage errors in the JPL RL05M GRACE mascon solution, Water Resour. Res., 52, 7490-7502, 10.1002/2016WR019344, 2016.

Xie, H., Longuevergne, L., Ringler, C., and Scanlon, B. R.: Integrating groundwater irrigation into hydrological simulation of India: Case of improving model representation of anthropogenic water use impact using GRACE, Journal of Hydrology: Regional Studies, 29, 100681, 10.1016/j.ejrh.2020.100681, 2020.

Zhang, X., Wan, H., Zwiers, F. W., Hegerl, G. C., and Min, S.-K.: Attributing intensification of precipitation extremes to human influence, Geophysical Research Letters, 40, 5252–5257, 10.1002/grl.51010, 2013.

Acknowledgements

M.S. and R.T. acknowledge support from NERC-ESRC-DFID UPGro '*GroFutures*' (Ref. NE/M008932/1; www.grofutures.org); R.T. also acknowledges the support of a Royal Society – Leverhulme Trust Senior Fellowship (Ref. LT170004).

Data Availability

Supplementary information is available for this paper as a single PDF file. Data generated and used in this study can be made available upon request to the corresponding author.

Tables and Figures

Table 1. Identification number, name and general location of the world's 37 large aquifer systems as provided in the WHYMAP database (https://www.whymap.org/). Mean climatic condition of each of the 37 aquifer systems based on the aridity index is tabulated.

WHYMAP aquifer no.	WHYMAP Aquifer name	Continent	Climate zones based on Aridity index	WHYMAP aquifer no.	WHYMAP Aquifer name	Continent	Climate zones based on Aridity index
1	Nubian Sandstone Aquifer System	Africa	Hyper-arid	20	Maranhao Basin	South America	Humid
2	Northwestern Sahara Aquifer System	Africa	Arid	21	Guarani Aquifer System (Parana Basin)	South America	Humid
3	Murzuk-Djado Basin	Africa	Hyper-arid	22	Arabian Aquifer System	Asia	Arid
4	Taoudeni-Tanezrouft Basin	Africa	Hyper-arid	23	Indus River Basin	Asia	Semi-arid
5	Senegal-Mauritanian Basin	Africa	Semi-arid	24	Ganges-Brahmaputra Basin	Asia	Humid
6	Iullemmeden-Irhazer Aquifer System	Africa	Arid	25	West Siberian Artesian Basin	Asia	Humid
7	Lake Chad Basin	Africa	Arid	26	Tunguss Basin	Asia	Humid
8	Umm Ruwaba Aquifer (Sudd Basin)	Africa	Semi-arid	27	Angara-Lena Basin	Asia	Humid
9	Ogaden-Juba Basin	Africa	Arid	28	Yakut Basin	Asia	Humid
10	Congo Basin	Africa	Humid	29	North China Plains Aquifer System	Asia	Humid
11	Upper Kalahari-Cuvelai-Zambezi Basin	Africa	Semi-arid	30	Song-Liao Plain	Asia	Humid
12	Lower Kalahari-Stampriet Basin	Africa	Arid	31	Tarim Basin	Asia	Arid
13	Karoo Basin	Africa	Semi-arid	32	Paris Basin	Europe	Humid
14	Northern Great Plains Aquifer	North America	Sub-humid	33	East European Aquifer System	Europe	Humid
15	Cambro-Ordovician Aquifer System	North America	Humid	34	North Caucasus Basin	Europe	Semi-arid
16	California Central Valley Aquifer System	North America	Semi-arid	35	Pechora Basin	Europe	Humid
17	Ogallala Aquifer (High Plains)	North America	Semi-arid	36	Great Artesian Basin	Australia	Semi-arid
18	Atlantic and Gulf Coastal Plains Aquifer	North America	Humid	37	Canning Basin	Australia	Arid
19	Amazon Basin	South America	Humid				

795 **Table 2.** Variability (expressed as standard deviation) in GRACE-derived estimates of GWS
796 from 20 realisations (3 GRACE-TWS and an ensemble mean of TWS, and 4 LSMs and an
797 ensemble mean of surface water and soil moisture storage, and a snow water storage) and
798 their reported range of uncertainty (% deviation from the ensemble mean) in world's 37 large
799 aquifer systems.

WHYMAP aquifer no.	WHYMAP Aquifer name	Std. deviation in GRACE-GWS (cm)	Range of uncertainty (%)	WHYMAP aquifer no.	WHYMAP Aquifer name	Std. deviation in GRACE-GWS (cm)	Range of uncertainty (%)
1	Nubian Sandstone Aquifer System	1.05	83	20	Maranhao Basin	5.68	136
2	Northwestern Sahara Aquifer System	1.29	121	21	Guarani Aquifer System (Parana Basin)	3.37	77
3	Murzuk-Djado Basin	1.17	189	22	Arabian Aquifer System	2.01	163
4	Taoudeni-Tanezrouft Basin	0.99	193	23	Indus River Basin	3	78
5	Senegal-Mauritanian Basin	3.23	96	24	Ganges-Brahmaputra Basin	9.84	58
6	Iullemmeden-Irhazer Aquifer System	1.52	116	25	West Siberian Artesian Basin	7.53	79
7	Lake Chad Basin	2.23	91	26	Tunguss Basin	7.4	103
8	Umm Ruwaba Aquifer (Sudd Basin)	4.95	113	27	Angara-Lena Basin	3.73	48
9	Ogaden-Juba Basin	1.52	57	28	Yakut Basin	4.15	83
10	Congo Basin	5.09	98	29	North China Plains Aquifer System	3.93	77
11	Upper Kalahari-Cuvelai-Zambezi Basin	10.03	36	30	Song-Liao Plain	2.63	62
12	Lower Kalahari-Stampriet Basin	1.76	106	31	Tarim Basin	1.37	219
13	Karoo Basin	3.06	74	32	Paris Basin	4.06	84
14	Northern Great Plains Aquifer	4.18	111	33	East European Aquifer System	5.91	75
15	Cambro-Ordovician Aquifer System	4.56	44	34	North Caucasus Basin	4.67	66
16	California Central Valley Aquifer System	9.73	55	35	Pechora Basin	8.55	94
17	Ogallala Aquifer (High Plains)	4.05	104	36	Great Artesian Basin	2.77	69
18	Atlantic and Gulf Coastal Plains Aquifer	2.56	193	37	Canning Basin	5.34	57
19	Amazon Basin	10.93	58				

800

801

Main Figures:

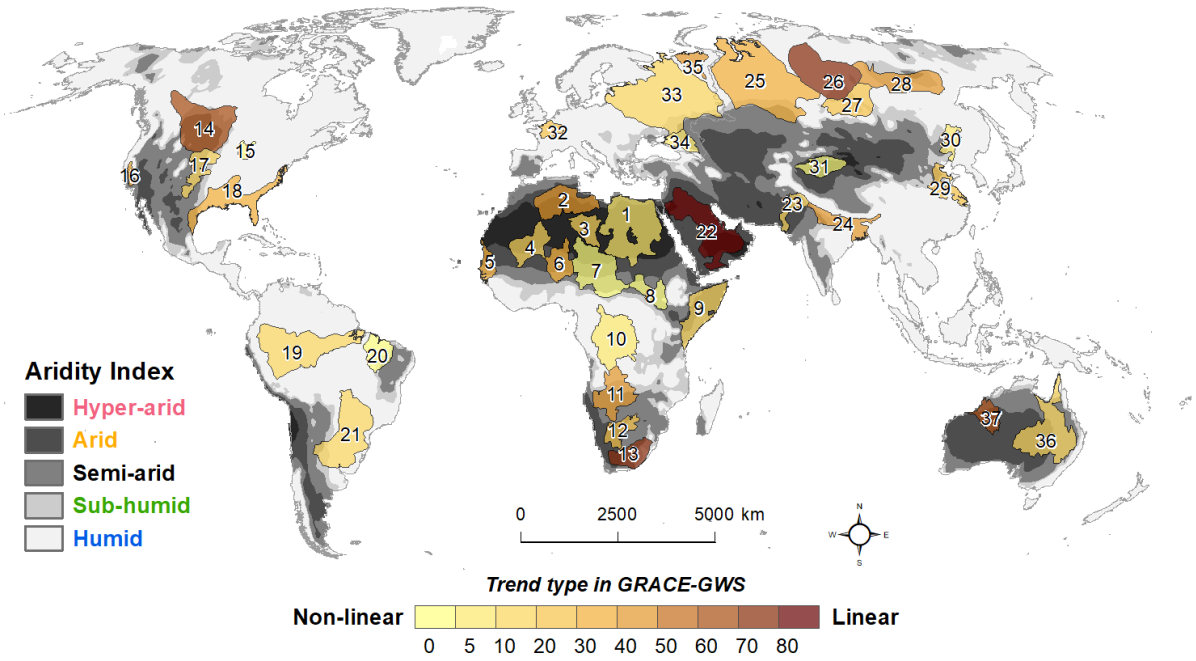

Fig. 1. Global map of 37 large aquifer systems from the GIS database of the World-wide Hydrogeological Mapping and Assessment Programme (WHYMAP); names of these aquifer systems are listed in Table 1 and correspond to numbers shown on this map for reference. Grey shading shows the aridity index based on CGIAR's database of the Global Potential Evapo-Transpiration (Global-PET) and Global Aridity Index (https://cgiarcsi.community/); the proportion (as a percentage) of long-term trends in GRACE-derived ΔGWS of these large aquifer systems that is explained by linear trend fitting is shown in colour (i.e. linear trends toward red and non-linear trends toward blue).

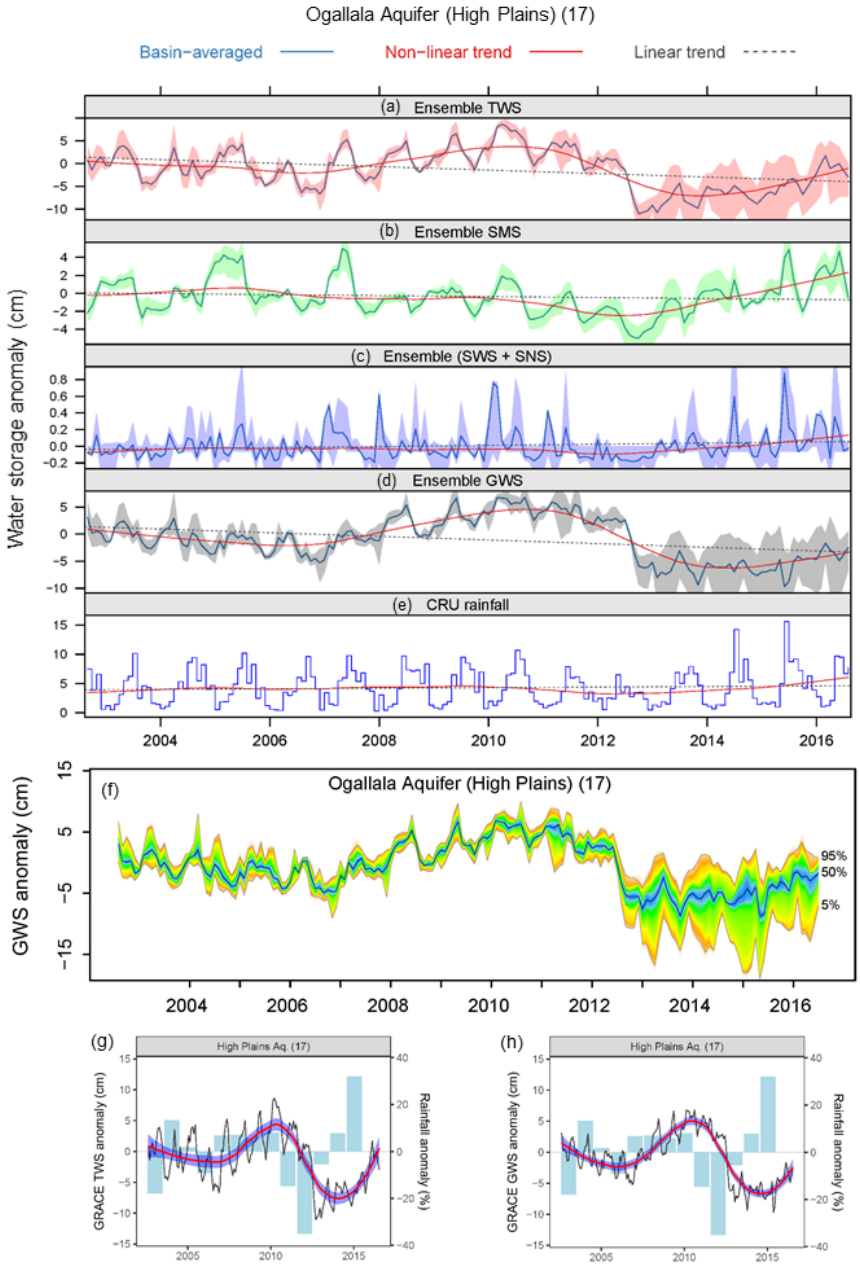

Fig. 2. Time-series data of terrestrial water storage anomaly (ΔTWS) from GRACE and individual water stores from GLDAS Land Surface Models (LSMs): (a) Ensemble monthly GRACE ΔTWS from three solutions (CSR, Mascons, GRGS), (b-c) ensemble monthly ΔSMS and ΔSWS + ΔSNS from four GLDAS LSMs (CLM, Noah, VIC, Mosaic), (d) computed monthly ΔGWS and (e) monthly precipitation from August 2002 to July 2016, (f) range of uncertainty in GRACE-derived GWS from 20 realisations, (g) ensemble TWS and annual precipitation, and (h) ensemble GRACE-derived GWS and annual precipitation for the High Plains Aquifer System in the USA (WHYMAP aquifer no. 17). Values in the Y-axis of the top four panels show monthly water-storage anomalies (cm) and the bottom panel shows monthly precipitation (cm). Time-series data (a-e) for the 36 large aquifer systems can be found in supplementary Figs. S1-S36.

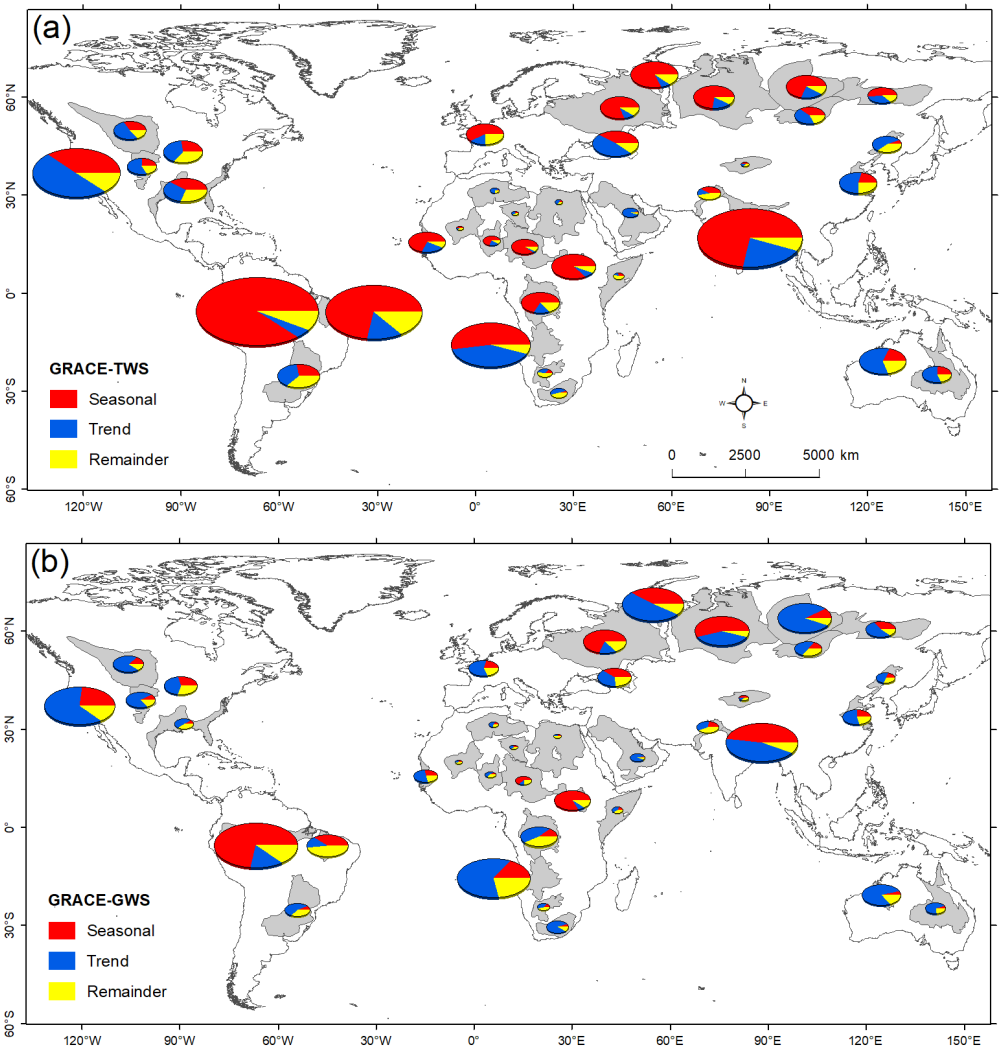

Fig. 3. Seasonal-Trend decomposition of (a) GRACE ΔTWS and (b) GRACE ΔGWS time-series data (2002 to 2016) for the world's 37 large aquifer systems using the STL decomposition method; seasonal, trend and remainder or irregular components of time-series data are decomposed and plotted as pie charts that are scaled by the variance of the time series in each aquifer system.

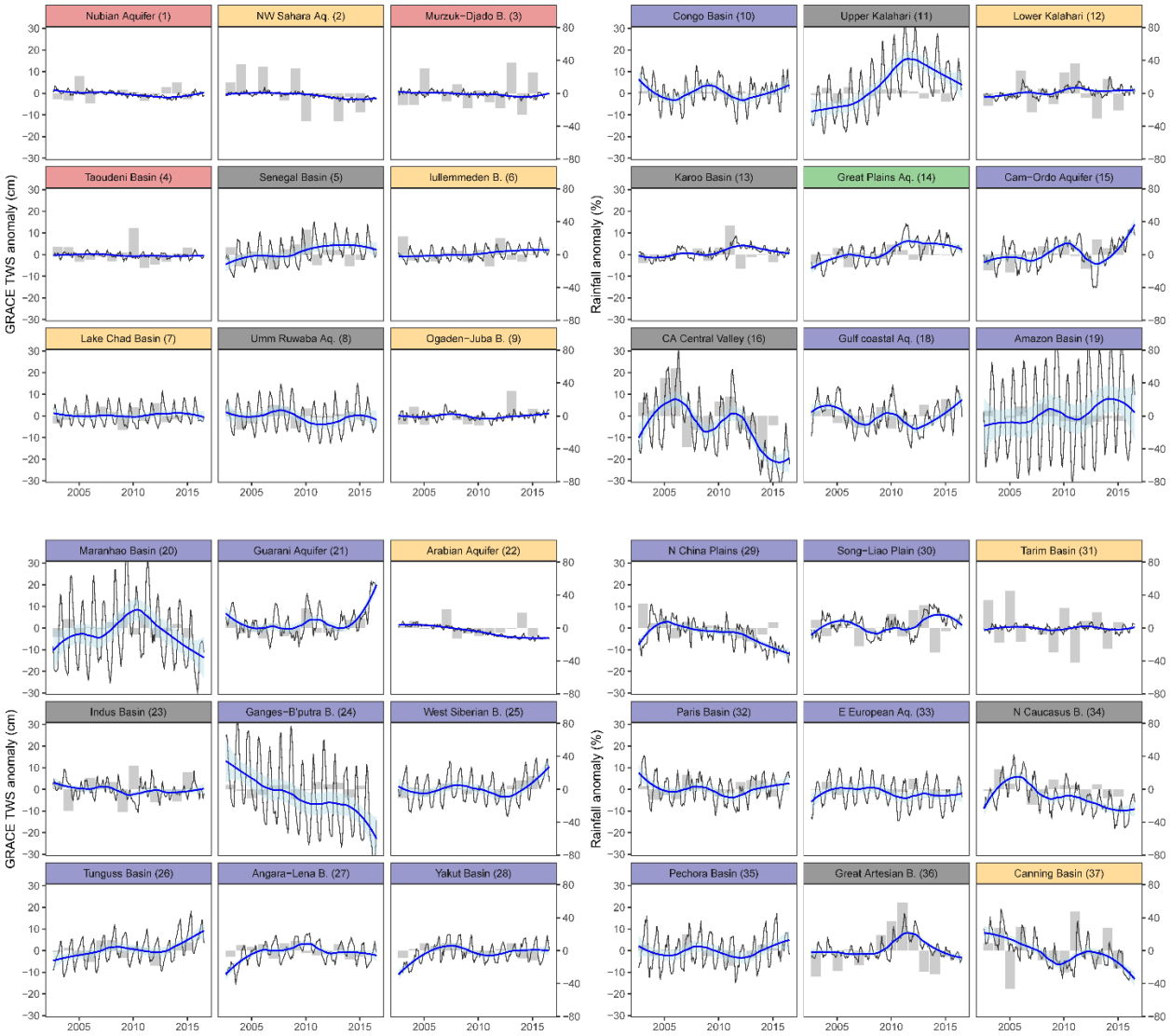

Fig. 4. Monthly time-series data (black) of ensemble GRACE ΔTWS for 36 large aquifer systems with a fitted non-linear trend line (Loess smoothing line in thick blue) through the time-series data; GRACE ΔTWS for the remaining large aquifer system (High Plains Aquifer System, (WHYMAP aquifer no. 17) is given in Fig. 2. Shaded area in semi-transparent cyan shows the range of 95% confidence interval of the fitted loess-based non-linear trends; light grey coloured bar diagrams behind the lines on each panel show annual precipitation anomaly (i.e., percentage deviation from the mean precipitation for the period of 1901 to 2016); banner colours indicate the dominant climate of each aquifer based on the mean aridity index shown in the legend on Fig. 1.

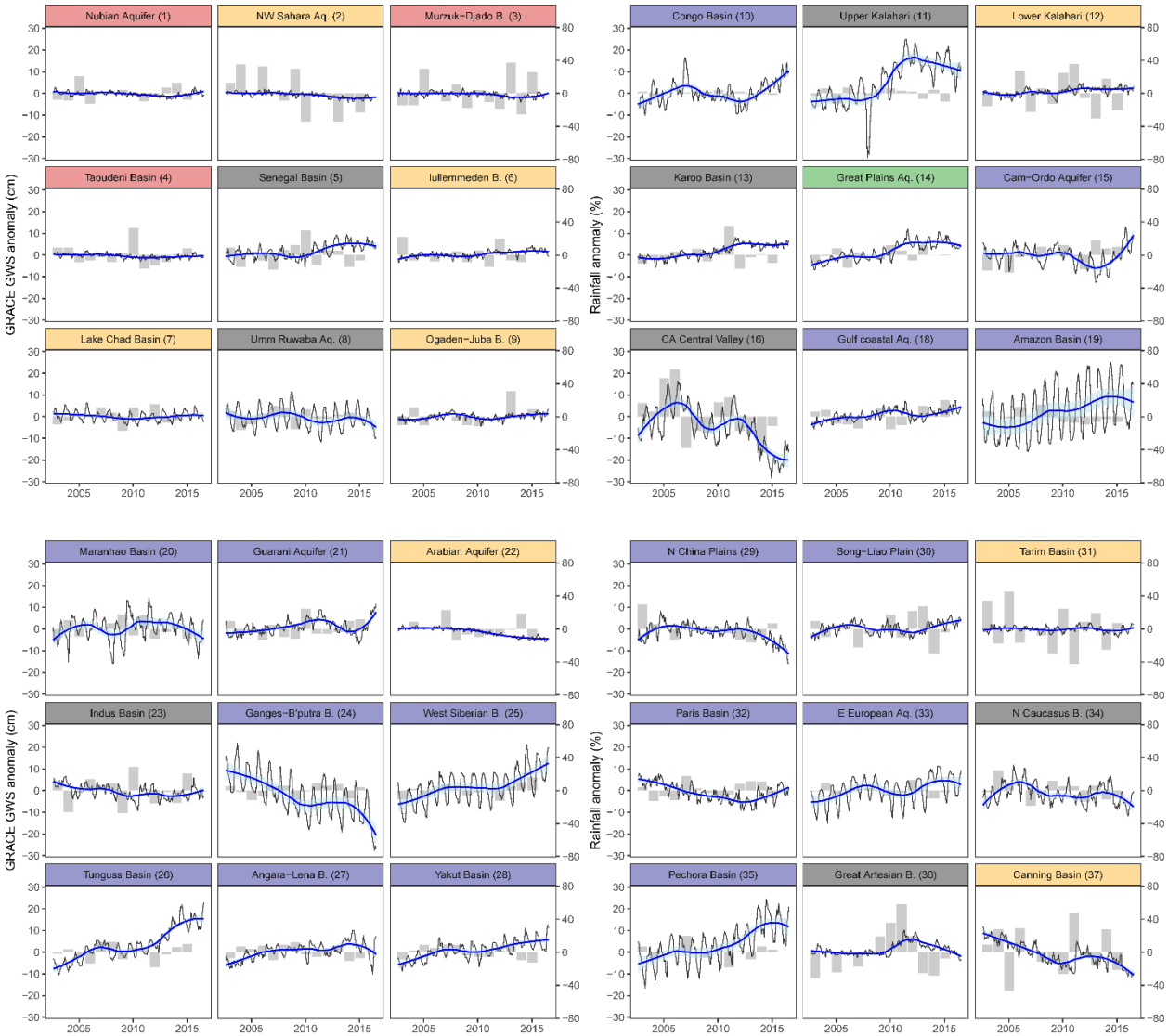

Fig. 5. Monthly time-series data (black) of ensemble GRACE ΔGWS for 36 large aquifer systems with a fitted non-linear trend line (Loess smoothing line in thick blue) through the time-series data; GRACE ΔGWS for the remaining large aquifer system (High Plains Aquifer System, (WHYMAP aquifer no. 17) is given in Fig. 2. Shaded area in semi-transparent cyan shows the range of 95% confidence interval of the fitted loess-based non-linear trends; light grey coloured bar diagrams behind the lines on each panel show annual precipitation anomaly (i.e., percentage deviation from the mean precipitation for the period of 1901 to 2016); banner colours indicate the dominant climate of each aquifer based on the mean aridity index shown in the legend on Fig. 1.

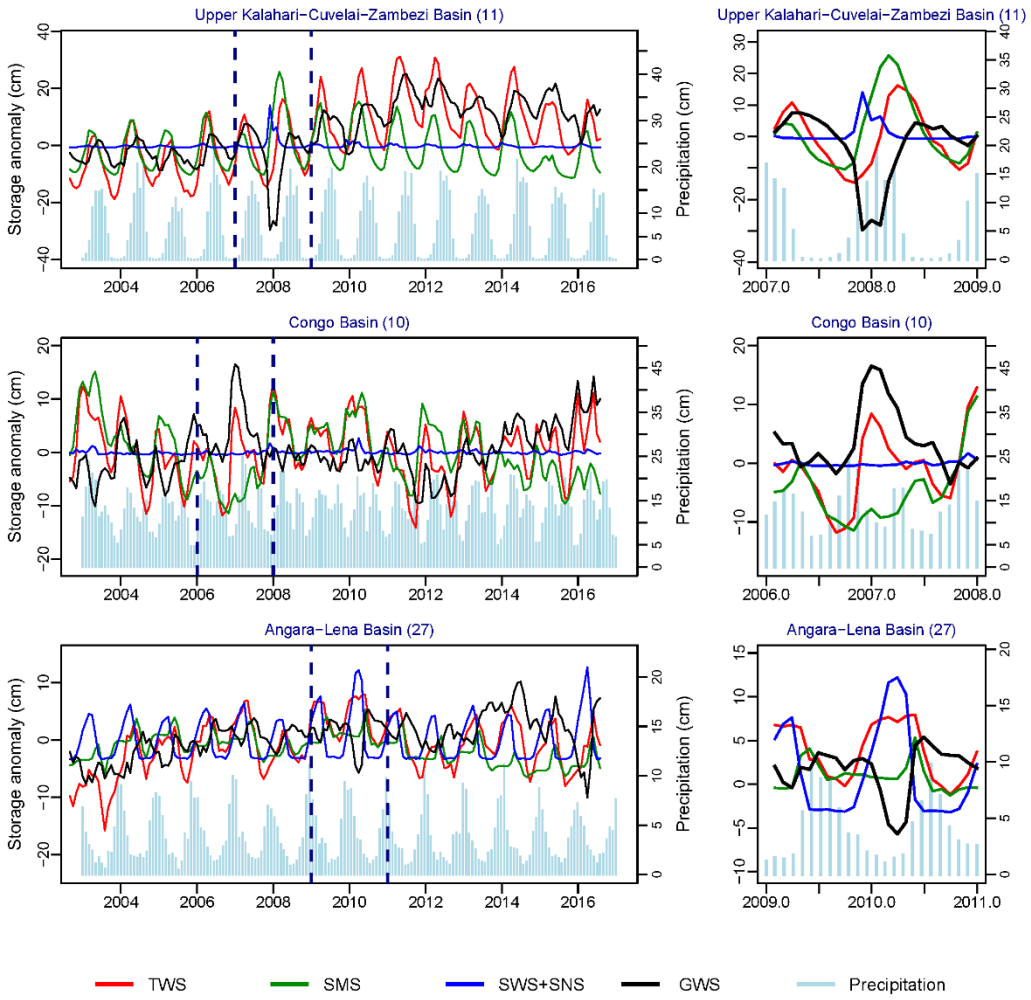

Fig. 6. Time series of ensemble mean GRACE ΔTWS (red), GLDAS ΔSMS (green), ΔSWS+ΔSNS (blue) and computed GRACE ΔGWS (black) showing the calculation of anomalously negative or positive values of GRACE ΔGWS that deviate substantially from underlying trends. Three examples include: (a) the Upper Kalahari-Cuvelai-Zambezi Basin (11) under a semi-arid climate; (b) the Congo Basin (10) under a tropical humid climate; and (c) the Angara-Lena Basin (27) under a temperate humid climate; examples from an additional five aquifer systems under semi-arid and arid climates are given in the supplementary material (Fig. S75).

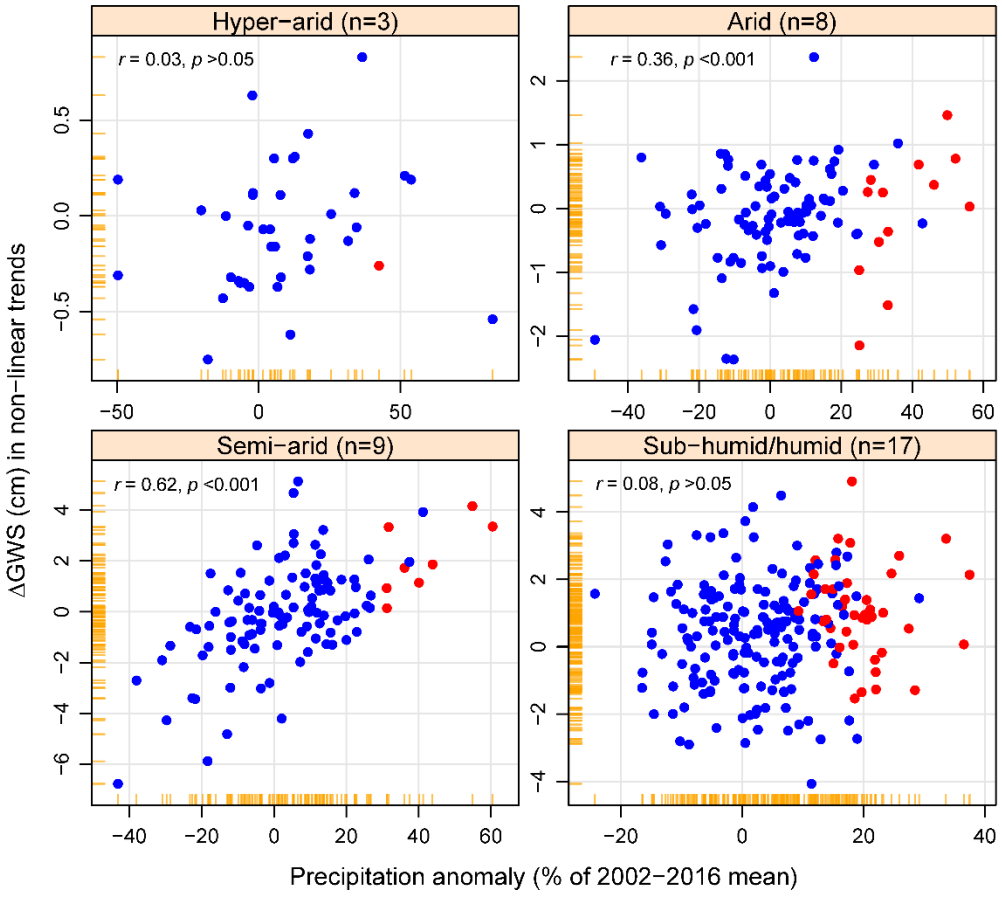

Fig. 7. Relationships between precipitation anomaly and annual changes in non-linear trends of GRACE ΔGWS in the 37 large aquifer systems grouped by aridity indices; annual precipitation is calculated based on hydrological year (August to July) for 12 of these aquifer systems and the rest 25 following the calendar year (January to December); the highlighted (red) circles on the scatterplots are the years of statistically extreme (>90th percentile; period: 1901 to 2016) precipitation.

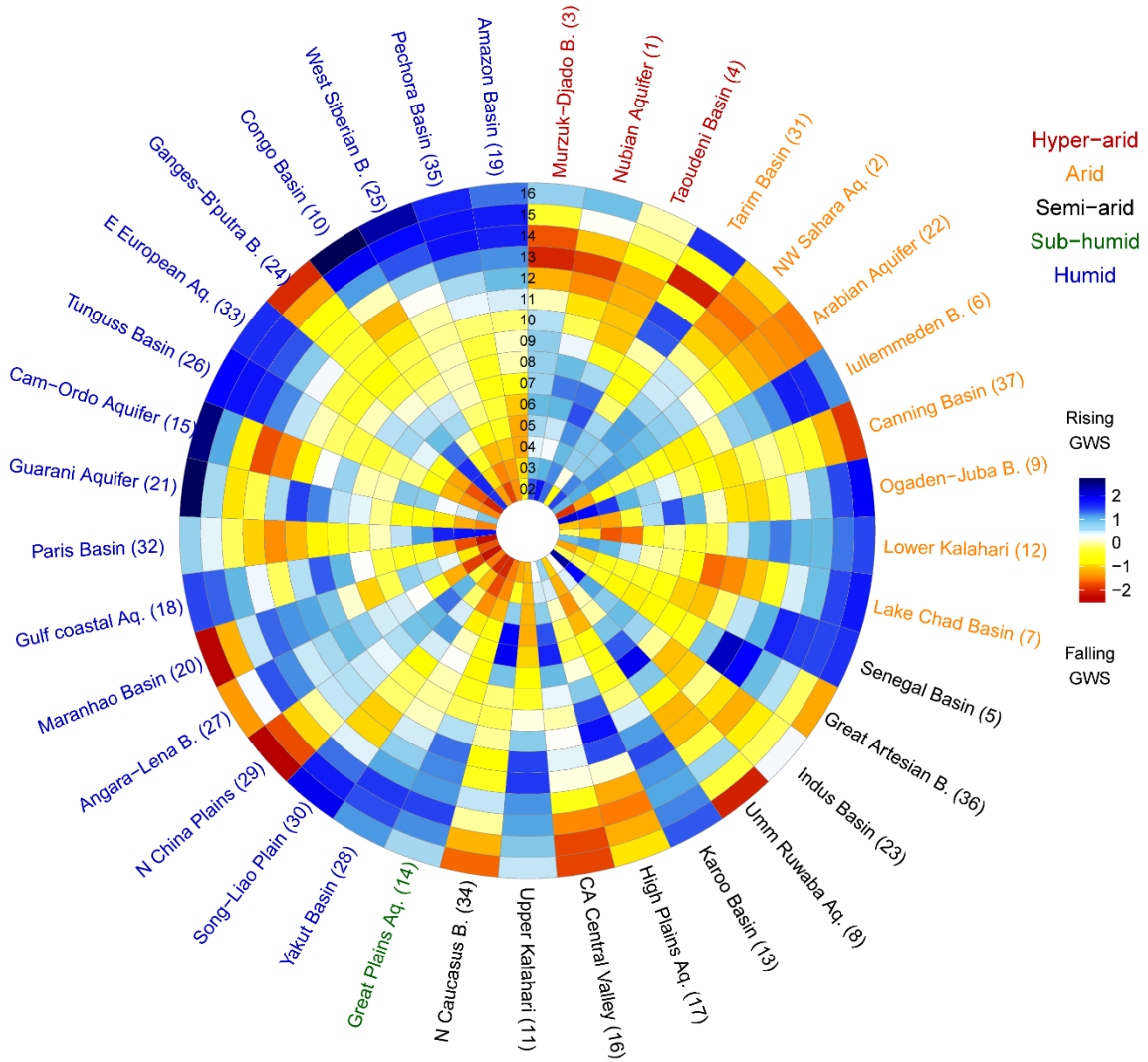

Fig. 8. Standardised monthly anomaly of non-linear trends of ensemble mean GRACE ΔGWS for the 37 large aquifer systems from 2002 to 2016. Colours yellow to red indicate progressively declining, short-term trends whereas colours cyan to navy blue indicate rising trends; aquifers are arranged clockwise according to the mean aridity index starting from the hyper-arid climate on top of the circular diagram to progressively humid. Legend colours indicate the climate of each aquifer based on the mean aridity index; time in year (2002 to 2016) is shown from the centre of the circle outwards to the periphery.